In-Situ Analysis and Quantification of Swelling Kinetics in Glassy and Rubbery Networks Using ^1H and ^{19}F Magnetic Resonance Microscopies

George D. Cody* and Robert E. Botto

Chemistry Division, Argonne National Laboratory, 9700 South Cass Avenue, Argonne, Illinois 60439

*Received October 22, 1993; Revised Manuscript Received January 25, 1994**

ABSTRACT: ^1H and ^{19}F magnetic resonance microscopies are used to determine the characteristics of diffusion in four different network–solvent systems. Time-resolved analysis of the concentration profiles of toluene in polybutadiene and hexafluorobenzene in poly(methyl silicone) demonstrates that solvent transport in these systems is Fickian. The kinetics of solvent transport in two glassy networks, however, is shown to be non-Fickian. These latter two systems are characterized by sharp solvent fronts which propagate into the cores of the samples at a constant velocity. The swelling kinetics are quantified by applying a simple model which couples the kinetics of solvent diffusion to a second-order phase transition which induces network relaxation. Parameterization is accomplished with two kinetic terms and one thermodynamic parameter. These are a mass-fixed glassy diffusion coefficient, a network relaxation constant, and a critical concentration corresponding to the concentration of solvent necessary to induce a glass to rubber transition. Solvent from velocities, obtained through magnetic resonance microscopy, are used with independently derived critical concentrations to calculate the glassy diffusion coefficient and network relaxation rate constant. Kinetic swelling data are then fit with theoretical uptake curves computed using these parameters. A high-quality fit demonstrates that the proposed model successfully quantifies non-Fickian transport using a small number of physically based dynamic parameters.

Introduction

The phenomenological aspects of solvent transport into polymers have fascinated researchers for decades. In addition to stimulating interest in terms of basic science issues, an understanding of mass transport behavior in polymer systems is also a benefit to industrial and manufacturing applications such as solvent stripping following casting, development of drug delivery systems and photoresist polymers, and prediction of polymer degradation, as well as numerous others. In order to predict long-term performance capabilities or to optimize short-term residence times in a given process stream, it is crucial that solvent transport behavior be both quantifiable and predictable in terms of the chemical and physical structural characteristics of the network.

Significant insight into the character of solvent transport has been obtained through time-resolved, direct imaging of concentration gradients during solvent uptake. Early on, optical microscopic methods revealed that solvent transport in some macromolecular networks did not conform to Fickian kinetics.[1] Specifically, these systems exhibited steep-gradient solvent fronts which propagate into a sample at a constant velocity, much like a shock wave; such behavior has been called case II transport to distinguish it from Fickian transport. Subsequent analyses of concentration profiles observed during solvent transport, in a wide variety of network–solvent systems, has been accomplished using X-ray absorption,[2] Rutherford backscattering,[3,4] and, recently, NMR imaging.[5–8] Each technique has helped to reveal the fundamental characteristics of case II transport.

Case II transport is not restricted to synthetic polymers. Biopolymers and geopolymers such as cellulose and bituminous coals, for example, also exhibit case II transport behavior under suitable conditions.[1,9,10] All that is required for case II transport is that the dry network exist initially in a glassy state and that the penetrating solvent is capable of suppressing T_g.

Given the interesting physical behavior of glassy networks near their glass transition, the search for a theoretical basis for non-Fickian behavior has been irresistible for both experimentalists and theorists. To date, numerous theories abound.[11–19] While the specific approaches to this problem vary from one model to another, universally they rely on the generality that case II behavior results from coupled solvent diffusion and network relaxation.[20,21] There are several rigorous approaches which quantify case II transport in terms of a relatively small set of physically based dynamic parameters.[14–19] These models tend to be valid only for very small displacements from equilibrium, because linear behavior of the governing equations is required in order to obtain an analytical solution. Large-scale departures from equilibrium conditions require that the concentration dependence on each of the dynamic parameters be considered explicitly. This has resulted in a complicated data analysis, stemming from a many-fold expansion of the parameter set and, consequently, an increase in the total number of degrees of freedom of the model.

Many, if not most, applications involving solvent–macromolecular systems are far from equilibrium. In the present paper, the essential characteristics of case II transport are exploited for the purpose of reducing the dynamic parameter set size, in order to simplify quantification under conditions far from equilibrium, e.g., the situation of solvent transport following immersion of a dry macromolecular network into a solvent reservoir. Case II transport of methanol in poly(ethyl methacrylate) (PEMA) and pyridine in coal is explored and compared with Fickian transport of toluene in polybutadiene rubber (PBD) and hexafluorobenzene in poly(methyl silicone) (PMS) using magnetic resonance microscopy and optical microscopy.

* Abstract published in *Advance ACS Abstracts*, March 15, 1994.

0024-9297/94/2227-2607$04.50/0

Experimental Section

Samples and Preparation. Fine beads of high molecular weight ($M_w = 2.8 \times 10^5$) poly(ethyl methacrylate) (PEMA) were hot pressed into disks. PEMA has a glass transition at approximately 35 °C. Although it is only marginally soluble in methanol, a small degree of solvent-induced dilation is sufficient to suppress this transition to below room temperature. In the fully swollen state, PEMA exhibits pronounced viscoelastic behavior consistent with a transient network composed of highly entangled polymer strands. The volume fraction of PEMA fully dilated in methanol is on the order of 0.70.

In addition to this conventional glassy polymer, a sample of high-volatile bituminous coal (vitrain) was also selected. Although the chemistry of coal is enormously complex, its physical behavior is fairly simple.[22] At room temperature it exists in a glassy state, but a glass transition temperature on the order of 400 °C[23] has been suggested. Furthermore, various solvents have been reported to have the capability to suppress coal's glass transition temperature to below room temperature.[24] In the present experiment pyridine was chosen as the swelling solvent. The volume fraction of coal fully dilated in pyridine is on the order of 0.45. Samples were obtained by sectioning with a wafer saw and further reduced with a scalpel. Prior to initial swelling, the samples were thoroughly extracted in pyridine to remove any occluded soluble material.

In addition to the glassy networks, two samples of rubbery materials were analyzed: a sample of vulcanized polybutadiene rubber (PBD) dilated in toluene and a sample of lightly crosslinked poly(methyl silicone) (PMS) swollen in hexafluorobenzene. Both specimens were acquired from commercial suppliers. These samples were included for comparative purposes because both exist in a rubbery state throughout a solvent uptake experiment. In the fully dilated state, the volume fraction of toluene in the polybutadiene rubber is on the order of 0.35. The volume fraction of hexafluorobenzene in poly(methyl silicone) is on the order of 0.50.

Magnetic Resonance Microscopy of Solvent Transport. Time-resolved NMR images of the spatial distribution of solvent in each network were obtained at a field strength of 2.35 T, using a Techmag NMR Kit II and Libra data acquisition system based on a Macintosh Quadra 950 computer, and a home-built imaging probe[25] tuned to either a proton resonance frequency of 100.13 MHz or to the ^{19}F resonance frequency at 94.18 MHz. Three 1000-W Techron audio amplifiers drive three orthogonal linear magnetic field gradients on the order of 30 G/cm across the sample. Limiting factors in obtaining high-quality, time-resolved images are the overall spin density which determines the theoretical maximum signal intensity, the magnitude of the spin–lattice relaxation time, T_1, which limits the recycle delay, and the magnitude of homogeneous spin–spin relaxation time, T_2, which limits resolution given the constraint of time.

The characteristic relaxation times for each solvent–network system were established at full dilation using a standard inversion-recovery pulse sequence to derive T_1, and a Hahn spin-echo sequence to derive T_2. It is acknowledged that, in protonated solvent systems, contributions to the signal intensity can arise from both the protons in the solvent and protons associated with the mobile network. Analysis of the NMR spectral and dynamic characteristics of these swollen networks in deuterated solvents reveals that, in general, only a minor contribution to the total signal intensity results from the mobile network protons. This contribution is significant, however, in the case of PBD in toluene, as is demonstrated below. No signal is detectable from the rigidly bound protons in the glassy regions of PEMA or coal due to severe dipolar broadening (line width > 20 kHz) in the rigid solid. Obviously, in the case of ^{19}F imaging of solvent transport into poly(methyl silicone), the signal is derived from the solvent exclusively. Values for the various dynamic parameters are presented in Table 1.

In the present experiments, two-dimensional (2D) images are sufficient to elucidate the fundamental aspects of the transport phenomena. In order to ensure that the transport process was also two-dimensional, the upper and lower sample surfaces were protected from solvent infiltration by glass cover slips which restricted the flow of solvent to cross only the exposed faces of each sample. Each sample is rectangular with initial dimensions on the order of (1–2) × 1 mm. The experimental protocol involved immersing the sample in the solvent for a period of time, removing it from the solvent bath, acquiring an image, and reimmersing it. During the imaging stage the sample was placed in a cell with "plugs" such that the free volume within the cell was minimized. It was anticipated that this would reduce the amount of desorption over the duration of the imaging.

Table 1. Solvent–Network Characteristics

sample	solvent	T_g	Q^a	T_1 (ms)	T_2 (ms)
poly(methyl silicone)	hexafluorobenzene	$\ll T_{rt}$	2.0	300	2.0
polybutadiene	toluene	$\ll T_{rt}$	2.8	120	2.0
poly(ethyl methacrylate)	methanol	308 K	1.4	130	1.4
bituminous coal	pyridine	673 K	2.3	60	1.6

[a] Volumetric dilation ratio corresponding to equilibrium swelling at solvent activity $a = 1.0$.

In order to obtain sufficiently high quality images, given the dynamic behavior of the three protonated solvent–macromolecule systems, it was necessary to acquire 24 (128-point) transients with a recycle delay of 200 ms for each of 128 phase-encoded gradient positions using a standard imaging spin-echo pulse sequence.[26] This yielded reasonably high quality 2D images, with a resolution on the order of 70 μm, which was obtained over intervals of approximately 10 min. Typically a 130-kHz spectral width was chosen, establishing an echo time on the order of 0.5 ms. In the case of ^{19}F imaging, a longer T_1 and an inherently lower sensitivity of the nucleus necessitated the acquisition of 32 scans per phase-encoded position and a recycle delay of 500 ms; this resulted in a time interval on the order of 30 min to obtain a quality image. It is clear that during the time that the images are acquired some spatial averaging does take place. However, in all cases, the entire uptake process takes between 3 and 4 h, and therefore, it is assumed that the averaging is relatively minor. In terms of contributing to the overall uncertainty of the true spatial distribution of solvent molecules, this averaging may be less significant than T_2 weighting effects as is discussed below.

Optical Microscopic Measurement of Solvent-Induced Dilation. In addition to monitoring the 2D transport phenomena using NMR microscopy, continuous dilation measurements were also made on each solvent–network system using an optical microscope with transmitted light and low numerical aperture optics at 25× magnification. These data, obtained essentially instantaneously, are not compromised by time averaging effects.

Model for Case II Solvent Transport. From the outset, the goal was to design a simplified transport model which incorporates the essential characteristics of solvent swelling in systems which exhibit a glass transition accompanying solvent uptake. Any useful model constitutes a balance between the need to accurately describe a physical process and the desire to remain simple enough so as to reduce the degrees of freedom to a minimum number of crucial parameters. Ideally, these parameters should have a direct connection to fundamental molecular scale characteristics of the network.

Solvent-induced dilation of a macromolecular network, in the glassy and/or the rubbery states, results from osmotic stresses. Kinetically, the character of transport, hence dilation, is different in the two states. In the glassy state the characteristic time for solvent diffusion is very long relative to the time scale of molecular motions associated with the response of the network to the osmotic stress. In the rubbery state, however, diffusion is very rapid relative to network relaxation. The point of inversion in the respective behaviors occurs when the phase boundary from the glassy to the rubbery state is crossed.

Transport in the Glassy Concentration Region. Because solvent diffusion is assumed to be rate limiting in the glassy region, the initial stages of solvent transport are governed by essentially Fickian processes. Volume changes associated with swelling, however, indicate that bulk (convective) flow of solvent accompanies diffusion.[27] A particularly appealing approach to this type of swelling behavior was introduced by Tanaka et al.,[28] who consider the problem in a mass-fixed reference frame.

The essence of the approach is to consider the kinetics of solvent swelling in viscoelastic terms. The dilational strain which accompanies solvent penetration is defined through the time-dependent evolution of the displacement vector $\mathbf{u}(r,t)$, where $\mathbf{u}$ represents the displacement of a given point, r, at a time, t, from the strained to the equilibrium, or relaxed, condition. The differential equation that describes the time evolution of the displacement vector is given by Newton's second law:

$$\rho\, \partial^2\mathbf{u}/\partial t^2 = \text{div}\ \sigma - f\, \partial\mathbf{u}/\partial t \tag{1}$$

where the mass (ρ) times the acceleration term is given on the left, and the forces (the divergence of the stress tensor and a frictional force, where f is the friction coefficient related to friction between the solvent and the macromolecule) are given on the right side of eq 1. As noted by Tanaka and Fillmore,[29] under conditions of solvent swelling the frictional forces are far greater than the inertial terms. Accordingly, eq 1 can be simplified to

$$\partial\mathbf{u}/\partial t = \text{div}\ \sigma/f \tag{2}$$

The stress tensor is related to strain through the stress associated with the volume change and the stress which results from shear deformation. This is given in the usual way[30] in the equation

$$\sigma_{ij} = K\ \text{div}\ u_j\delta_{ij} + 2G(u_{ij} - (1/3)\ \text{div}\ u_j\delta_{ij}) \tag{3}$$

where

$$u_{ij} = (1/2)(\partial u_j/\partial x_i + \partial u_i/\partial x_j)$$

In eq 3, K is the osmotic bulk modulus, G is the osmotic shear modulus, and δ_{ij} is the Kronecker delta ($\delta_{ij} = 1.0$ if $i = j$; otherwise $\delta_{ij} = 0$).

The initial application by Tanaka and Fillmore considered the system of polyacrylamide in water; this system is in a rubbery state throughout the swelling process. Dilation in the glassy state governed by Fickian transport is described by the same equations. In the polyacrylamide system it was shown that $K \gg G$, and so the furthermost right term in eq 3 was dropped in their treatment. It has been noted, however, that in some cases it was necessary to consider the full expression of eq 3.[31] At least in the earliest stages of swelling, K is also assumed to be much greater than G. In the present case, therefore, only the dilational terms in eq 3 will be considered.

The resulting expression for the time evolution of the displacement vector $\mathbf{u}$ during solvent swelling is then given by

$$\partial\mathbf{u}/\partial t = D_g\ \text{grad}(\text{div}\ \mathbf{u}) \tag{4}$$

where the cooperative diffusion coefficient, D_g, governs the dilation of the glassy network and is given by

$$D_g = K_{OS}/f \tag{5}$$

Any concentration dependence in D_g is derived from dependences on both the friction factor, f, and the osmotic modulus, K_{OS}. The magnitude of K_{OS} is related to solvent concentration through activity–composition relationships in the solvent–polymer system. By definition,[32] the osmotic modulus is given as

$$K_{OS} \equiv \phi_N(\partial\pi/\partial\phi_N) \tag{6}$$

where ϕ_N is the volume fraction of the network and π is the osmotic pressure. Given an equation of state for solvent–polymer systems along the lines of a typical lattice fluid,[33] it is seen that

$$K_{OS} \propto 1/(1 - \phi_N) \tag{7}$$

Asymptotic behavior of K_{OS} at $\phi_N = 1.0$ indicates the potential for an extremely large diffusion coefficient at extremely low concentrations. However, the friction factor, f, is presumably also large in glassy polymers at low solvent concentrations, and it should decrease rapidly with concentration. It is likely, therefore, that changes in $f(\phi_N)$ compensate for changes in $K_{OS}(\phi_N)$, resulting in D_g remaining essentially constant with variation in concentration. In the present model, D_g will be treated as invariant with concentration.

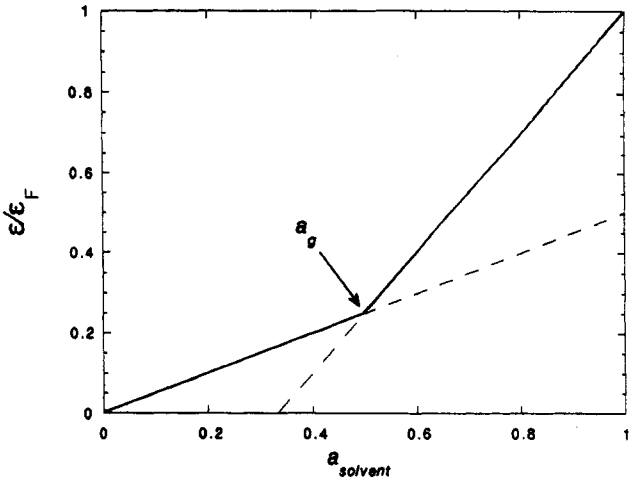

Figure 1. Relationship between hypothetical strain and solvent activity for a glassy solid which undergoes a glass transition at a solvent concentration given at a solvent activity of $a = a_g$. Strain is given normalized to the final strain in the rubbery state.

Glass to Rubber Transition. The transformation from a glass to a rubber is manifested in a significant increase in the magnitude of density fluctuations in the network resulting from an increase in the average contour length of cooperative segmental mobility. According to the free volume theory of glass to liquid transformations,[34] the glass transition temperature, T_g, defines the temperature at which the mobility of a given segment increases substantially due to an availability of sufficient free volume which exceeds some critical value. In a plot of volume vs temperature, T_g is identified as a discontinuity in the V–T slope, signifying a change in the coefficient of thermal expansion. Below T_g, large-scale segmental mobility is hindered; each segment is essentially trapped within a cage of surrounding segments. In the present experiments, solvent activity is analogous to temperature. Above some critical concentration, ϕ^* (corresponding to a critical activity, a_g), the probability of large-scale segmental displacement is greater than zero. Behavior analogous to V–T behavior is presented schematically in Figure 1, where solvent activity replaces temperature and normalized dilational strain (ϵ/ϵ_F) replaces molar volume. A discontinuity in the slope of ϵ/ϵ_F vs a at a_g would correspond to a solvent-induced second-order phase transition that is evident through a distinct change in the network pressure opposing dilation.

During swelling, solvent-induced crossing of the phase boundary allows the network to expand to a limit defined by the opposing, presumably entropic, elastic pressure associated with a rubbery macromolecular network. One of the principal assumptions of the present model is that the rate of expansion to this limit is not governed by diffusion of solvent. Rather, the expansion rate is governed purely by the viscoelastic response of the macromolecular network. Mathematically, this situation may be treated like the strain of a single Kelvin–Voigt viscoelastic element:

$$\epsilon(t) = \Pi J(1 - e^{-\alpha t}) + \epsilon^* \tag{8}$$

The strain at ϕ^* equals ϵ^*, where $\epsilon = \partial\mathbf{u}/\partial x$; Π is the osmotic pressure driving diffusion, and J is the network compliance. The relaxation rate constant α is given by the relationship

$$\alpha = K_R/\eta_1 \tag{9}$$

where η_1 is the bulk viscosity and K_R is the modulus of the swollen network.

The net effect of the relaxation at the glass to rubber transition is to convert the problem of solvent transport into a moving boundary value problem; the rate of relaxation in the rubbery region drives the diffusion in the glassy region.

In order to solve eq 4, initial and boundary conditions are required. The initial conditions are at $t = 0$ for each value of x_i. Accordingly,

$$\partial \mathbf{u}/\partial x_i = 0$$

While the boundary conditions, for $t > 0$, are given as $x_i = 0$,

$$\mathbf{u}(0) = 0.0$$

and at the edge of the network

$$\partial \mathbf{u}/\partial x_i = \Pi/K_G = \epsilon^*$$

where Π is the initial osmotic pressure corresponding to a solvent activity of zero and K_G is the glassy modulus. At the glass transition, K_G changes to K_R; the rate of change is given by the magnitude of α.

It now becomes a straightforward task to parameterize the swelling data. The effect of the variation of D_g, α, and ϕ^* on the swelling behavior can be shown using characteristic curves formulated in dimensionless units. Imbedded in the dimensionless time, τ, are the glassy diffusion coefficient and the half-length scale, L, given by

$$\tau = D_g t/L^2 \tag{10}$$

Dimensionless $\tilde{\alpha}$ is related to the actual relaxation rate constant α through the relation

$$\alpha = \tilde{\alpha} D_g/L^2 \tag{11}$$

The critical concentration ϕ^* is a fraction of the normalized dilation strain, given by eq 12, where ϕ_N° is the volume fraction of the network fully dilated in a given solvent. The problem as outlined was solved in two dimensions by the calculus of finite differences.

$$\phi^* = (1 - \phi_N^*)/(1 - \phi_N^\circ) \tag{12}$$

Figure 2D illustrates the time-dependent Fickian uptake behavior for comparison, i.e., without any glass to rubber transition and accompanying network relaxation. The initially linear uptake behavior, shown as normalized dilation vs the square root of dimensionless time (L/L_0 vs $\tau^{1/2}$), is characteristic of Fickian diffusion. In Figure 2A–C characteristic curves for various values of $\tilde{\alpha}$ and ϕ^* are presented; case II uptake behavior is clearly distinguishable from Fickian transport behavior.

Depending on the magnitude of $\tilde{\alpha}$, the characteristic shape of the uptake curve evolves from essentially concave upward at high values to sigmoidal at the lower values. The concave upward behavior reflects the nearly linear uptake behavior with time, consistent with what has been observed for case II behavior. The shape of the characteristic curves depends on the magnitudes of both $\tilde{\alpha}$ and ϕ^*. At low magnitudes of $\tilde{\alpha}$, the shape of the uptake curves varies substantially with the magnitude of ϕ^*; at moderate to large magnitudes of $\tilde{\alpha}$, however, the curves become topologically very similar. This means that the shape of the characteristic curve in the range of moderate to large $\tilde{\alpha}$ cannot be used to uniquely fix both parameters; therefore, additional information on either $\tilde{\alpha}$ or ϕ^* is required.

The shape of the concentration gradient is also diagnostic of the transport mechanism. Parts A–C of Figure 3 show the shapes of the solvent front calculated for various values of $\tilde{\alpha}$, with ϕ^* set, for example, at 0.25. The gradient associated with Fickian diffusion is exponential as depicted in Figure 3D. In the case of networks which undergo a transition of state to a rubber, a sharply defined solvent front results. The evolution from concave upward to a sigmoidal solvent front is a consequence of the magnitude of $\tilde{\alpha}$; a low value of $\tilde{\alpha}$ yields a sigmoidal front and a sigmoidal uptake curve.

The computed velocity of the solvent front, $\tilde{\nu}$, is constant through a range of $\tilde{\alpha}$ over 4 orders of magnitude and ϕ^* ranging from 0.05 to 0.75 of its final value. It can be shown that $\tilde{\nu}$ is a function of all three principal dynamic parameters; however, an analytical expression which relates D_g, $\tilde{\alpha}$, and ϕ^* to $\tilde{\nu}$ in this model has not been determined.

For example, increases in the magnitude of $\tilde{\alpha}$ increase the front velocity (Figure 4) as expected, since the relaxation drives the overall swelling process. However, as $\tilde{\alpha} \to \infty$, $\tilde{\nu}$ rapidly reaches an asymptotic limit, after which the velocity becomes purely a function of D_g and ϕ^*. The effect of increasing ϕ^* reduces the front velocity accordingly (Figure 5). Whereas this high degree of interdependence between the principal dynamic parameters precludes the use of ν alone to deduce their absolute magnitudes,

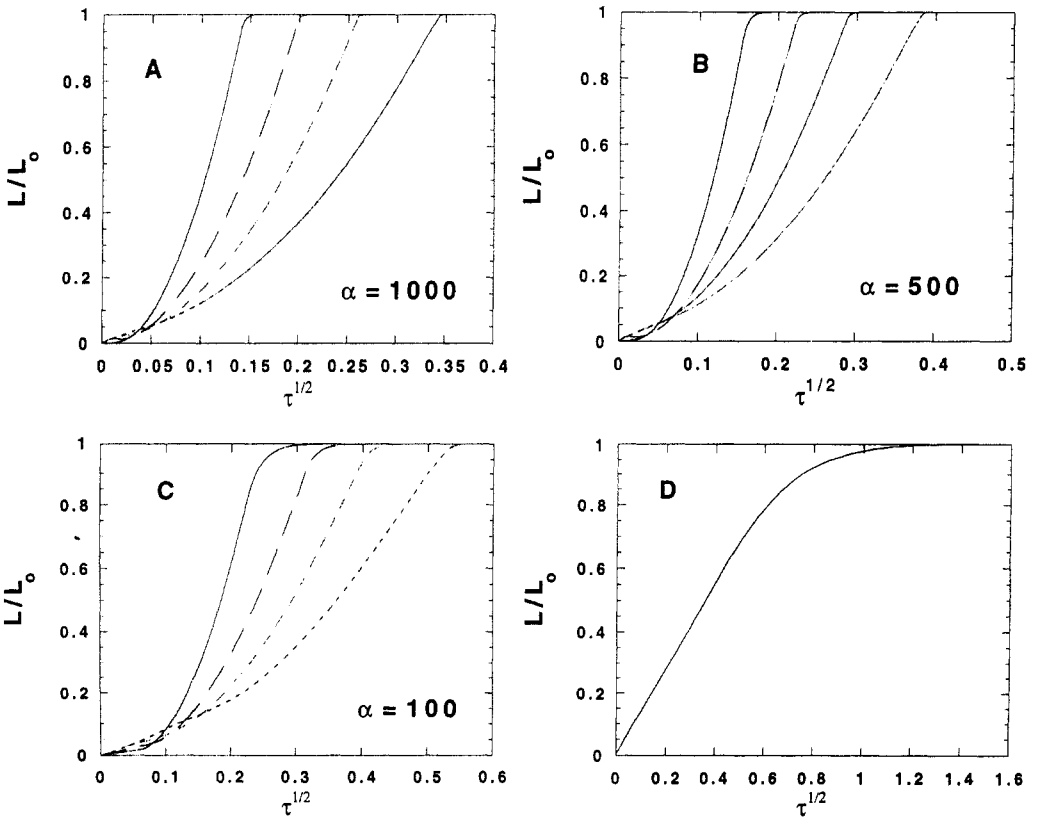

Figure 2. Calculated uptake curves plotting normalized dilation vs the square root of dimensionless time (τ). In (A)–(C), individual curves correspond to values of ϕ^* of 0.05, 0.25, 0.50, and 0.75, from left to right.

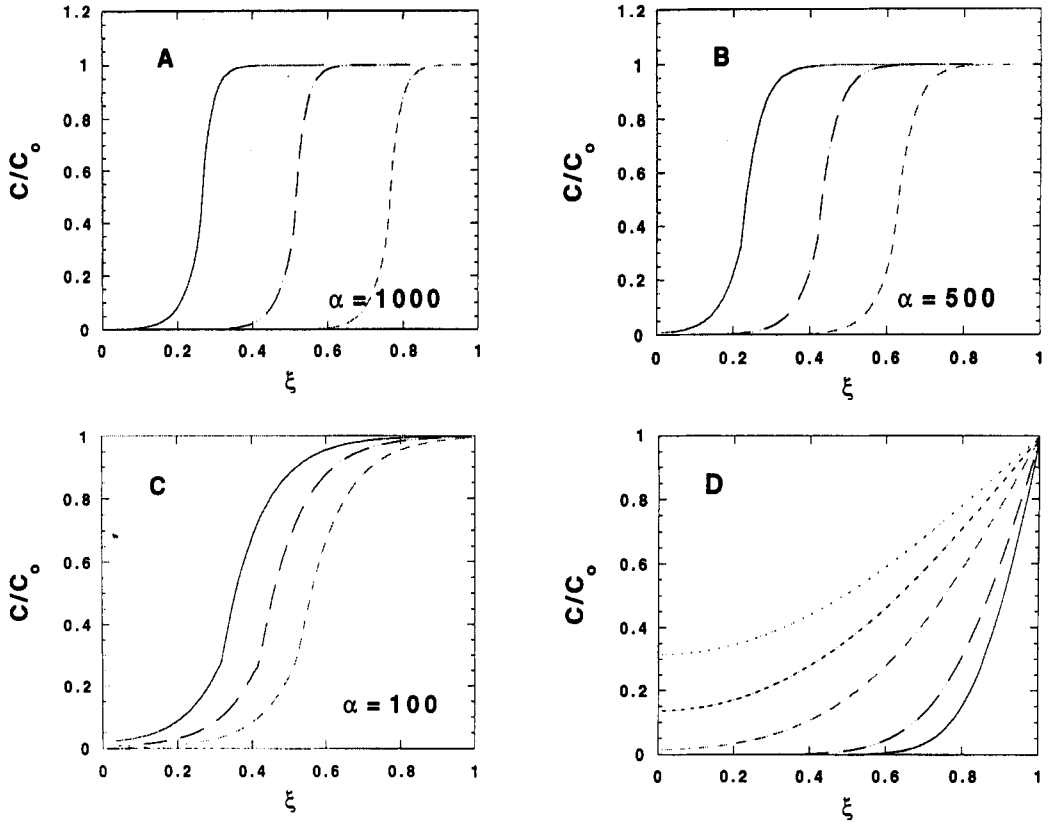

Figure 3. Solvent concentration gradients calculated for normalized concentration, C/C_0, as a function of normalized distance, $\xi = r/L$, for Fickian and non-Fickian transport. Non-Fickian transport is computed for different magnitudes of the dimensionless relaxation rate, α.

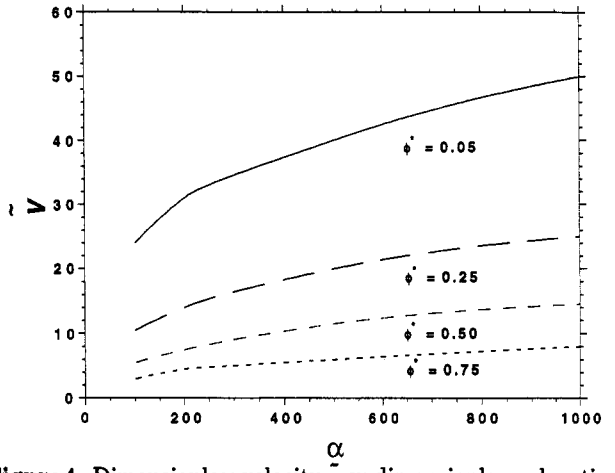

Figure 4. Dimensionless velocity, $\tilde{\nu}$, vs dimensionless relaxation rate, α, for values of 0.05, 0.25, 0.50, and 0.75 of the normalized critical concentration, ϕ^*.

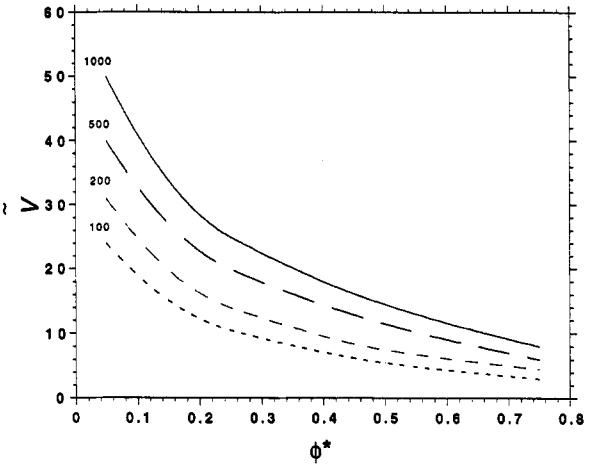

Figure 5. Dimensionless velocity, $\tilde{\nu}$, vs critical concentration, ϕ^*, for α = 100, 200, 500, and 1000.

the magnitude of ν together with some constraint on either $\tilde{\alpha}$ or ϕ^* is sufficient to quantify the uptake behavior (vide supra).

Results and Discussion

Examples of the results of magnetic resonance microscopy are presented in Figure 6. Figure 6A presents a 2D ^{19}F image projection of a specimen of poly(methyl silicone) swelling in hexafluorobenzene, observed at some intermediate time. Note the shallow concentration gradient into the core of the specimen. The 2D image of poly(ethyl methacrylate) in methanol (Figure 6B) is strikingly different; in this case a sharp front is observed with a nearly constant solvent concentration behind the front.

It is particularly useful to present the magnetic resonance microscopy data in the form of 1D slices, reconstructed from the center of the 2D image projections, Figure 7. Figure 7A presents sequential cross-sections through PBD dilated in toluene; a sizable contribution to the image intensity arises from the protons associated with the rubbery PBD itself. Superimposed on this is the additional signal due to the solvent. Clearly evident, however, are the smooth, exponential, solvent gradients directed into the core of the sample, indicating a Fickian transport mechanism. Fickian transport is similarly revealed in the case of the fluorinated solvent in PMS (Figure 7B). Recall that in this case the signal is due entirely to the solvent. Smooth solvent gradients are clearly evident despite the lower signal-to-noise ratios obtained in the ^{19}F images. Fickian behavior in these systems is entirely expected; nevertheless, it is important to demonstrate that NMR imaging data can clearly differentiate between the two transport mechanisms.

As seen in Figure 6B, the character of transport is drastically different for PEMA swollen in methanol. The presence of a sharp solvent front and solvent-absent core (Figure 7C) clearly indicates case II transport. This

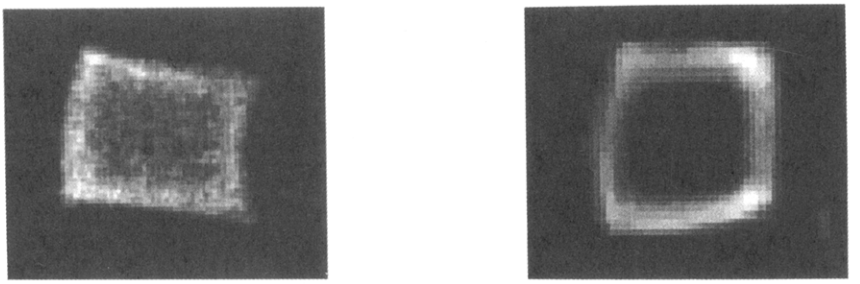

Polymethylsilicone - Hexafluorobenzene Polyethylmethacyrlate - Methanol

Figure 6. Transient 2D proton magnetic resonance images of (A, left) poly(methyl silicone) swelling in hexafluorobenzene and (B, right) poly(ethyl methacrylate) swelling in methanol.

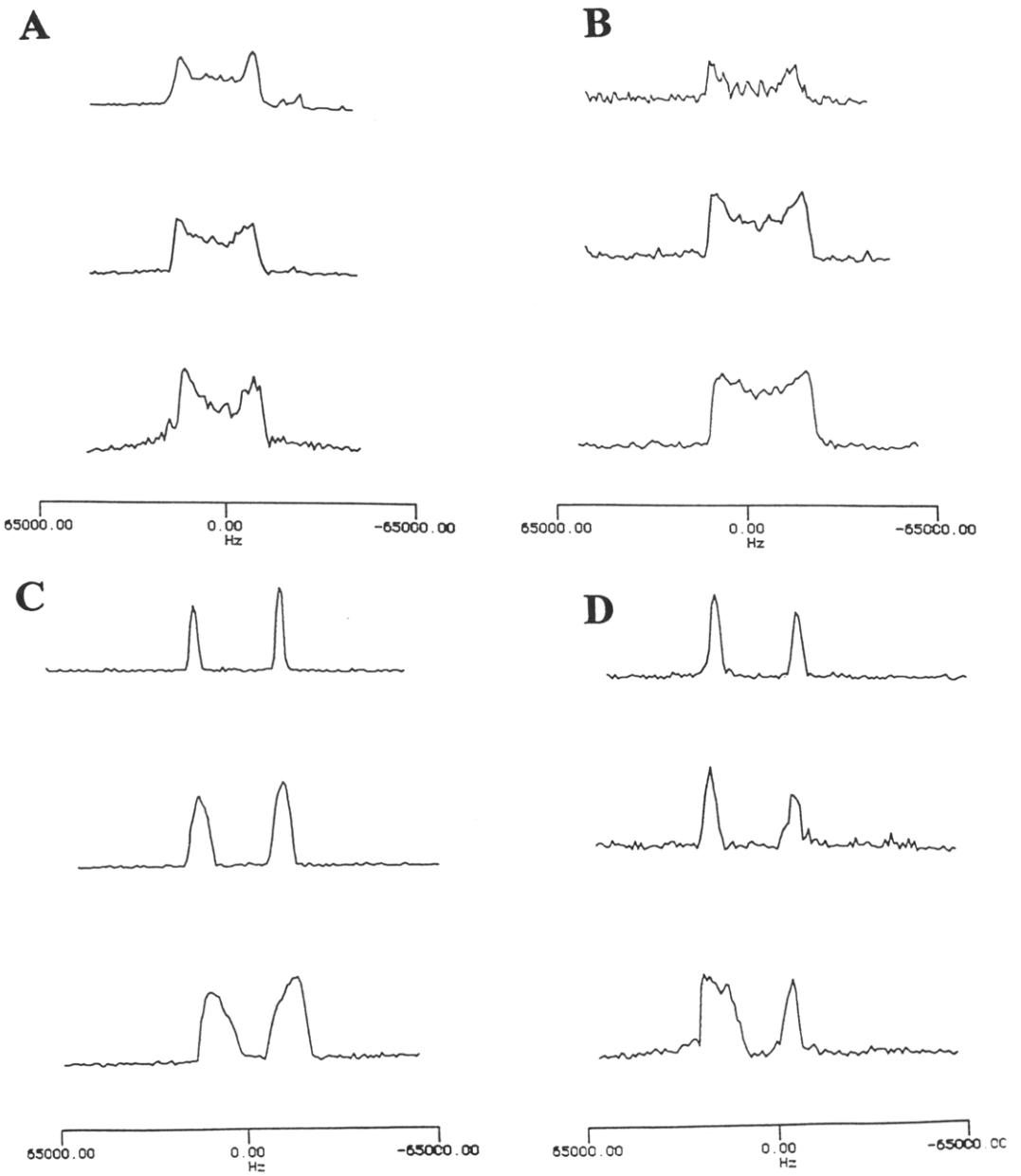

Figure 7. Time-evolved sequences of one-dimensional slices through 2D proton magnetic resonance images of (A) polybutadiene rubber (PBD) swollen in toluene, (B) poly(methyl silicone) rubber (PMS) swollen in hexafluorobenzene, (C) poly(ethyl methacrylate) (PEMA) swollen in methanol, and (D) bituminous coal swollen in pyridine.

behavior is typical of many acrylate polymers swollen in a variety of solvents, and it has been detected previously by NMR imaging techniques.[5-7] The imaging results give some indication of a sigmoidal solvent front similar to that derived numerically in Figure 3, and this suggests that the NMR images might be used to help constrain values of α. Pyridine transport in coal (Figure 7D) also exhibits case II behavior, whose signature is revealed by sharp solvent fronts moving into the sample. The situation was complicated by the formation of a crack on the left side of the lower most cross-section, which destroyed the symmetry of the solvent fronts. The formation of cracks

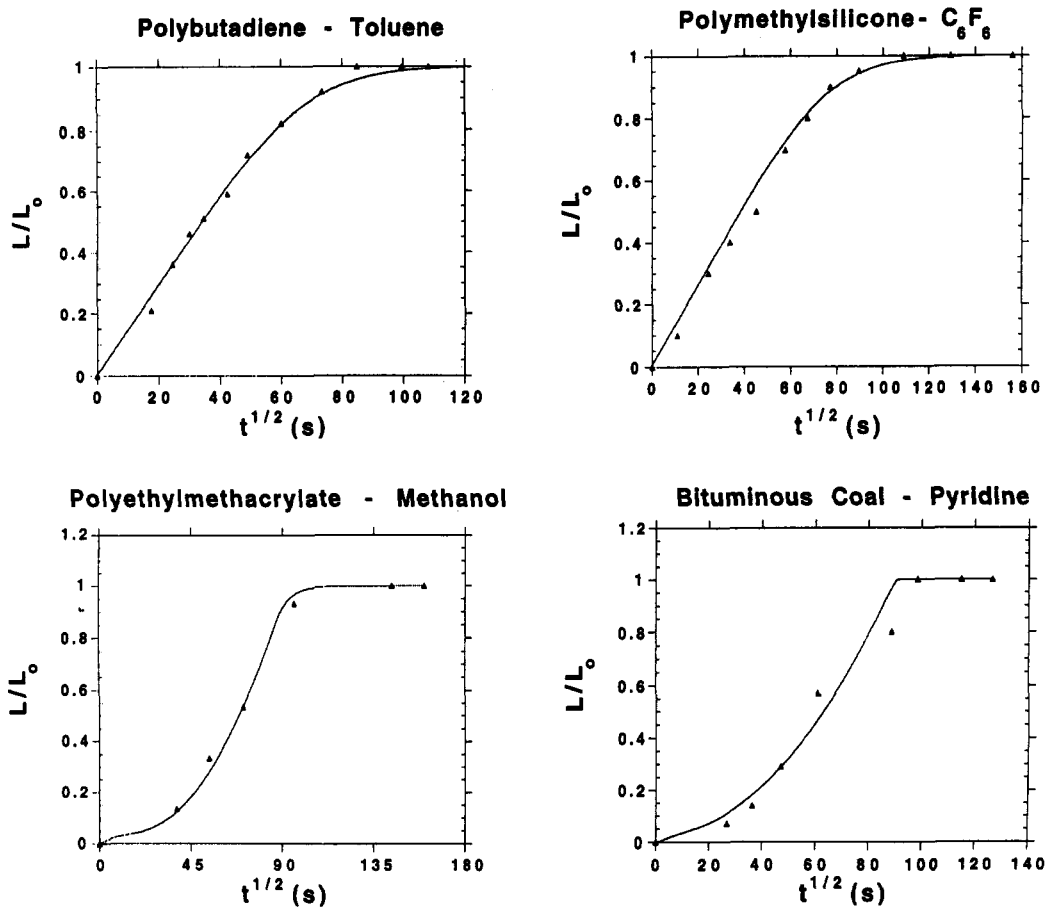

Figure 8. Experimental data and computed uptake curves for (A, top left) PBD swollen in toluene and (B, top right) PMS swollen in hexafluorobenzene fit to a 2D Fickian diffusion model and (C, bottom left) PEMA swollen in methanol and (D, bottom right) bituminous coal swollen in pyridine fit to a 2D non-Fickian diffusion model. Dynamic parameters are presented in Table 2.

Table 2. Dynamic Swelling Parameters Governing Solvent Uptake

sample	ϕ^*	v (μm/s)	$\tilde{\alpha}$	α (s^{-1})	$D_{S/R}$[a] (cm^2/s)
coal	0.61	5.4×10^{-2}	1500	1.3×10^{-2}	2.2×10^{-8}
PEMA	0.17	6.5×10^{-2}	80	8.8×10^{-4}	2.7×10^{-8}
PBD					2.6×10^{-6}
PMS					1.1×10^{-6}

[a] Diffusion coefficient derived for the glassy or rubbery state, as appropriate; see text.

accompanying case II transport is not unusual,[35] nor unexpected, considering the magnitude of the strain gradients along the solvent front.

The measured front velocities were constant for both the PEMA and the bituminous coal, consistent with case II transport. These data are presented in Table 2. There is some concern that a degree of spatial uncertainty or blurring may occur during evolution of the front within the imaging interval, leading to an apparent reduction in the gradient of the solvent front. Furthermore, distortions in image intensity due to T_2 effects are expected to add some further degree of uncertainty. The effect of T_2 weighting may be deduced through assumptions about the relationship between the mobility of solvent molecules in the macromolecular network and solvent concentration. It is expected that an exponential relationship exists between the viscosity of the solvent–network system and the concentration of the solvent; such relationships have been shown to be almost universal in rubbery polymers.[36] It is well known that T_2 is inversely proportional to viscosity. The net effect of T_2 weighting is to attenuate the signal at the solvent front, given a fixed spectral width and echo time optimized for a fully dilated network. This strong dependence of T_2 on solvent concentration may possibly result in the solvent gradient appearing sharper than that which actually exists. Clearly, there is some degree of uncertainty associated with the shape and position of the solvent front. The accuracy of the magnitudes of the front velocities derived from magnetic resonance microscopy, however, is not subject to these effects. Hence, the velocities provide a valuable and quantitative constraint for the parameterization of the uptake data.

Direct measurement of linear dilation accompanying swelling is a simple means to quantify the overall swelling behavior of rubbery networks.[29,30] Parts A and B of Figure 8 present linear dilation data for PBD and PMS in toluene and hexafluorobenzene, respectively, obtained using an optical microscope. These data are consistent with Fickian transport in rubbery networks, and they support observations using magnetic resonance microscopy (Figure 7A,B). Given the uptake data, it is trivial to derive a mass-fixed diffusion coefficient through linear fitting of the experimental data. The generation of a curve for Fickian transport, in the present case, requires solving the two-dimensional diffusion equation and integrating this solution with respect to time. Fitting of the dilation data results in values of $D_R = 2.5 \times 10^{-6}$ and 1.1×10^{-6} cm^2/s for PBD–toluene and PMS–hexafluorobenzene, respectively. These relatively large values of D_R reflect the high degree of inter- and intramolecular mobility of these networks, which explains the rapidity with which the rubbery systems respond to applied stresses that are osmotic in nature.

There are several degrees of freedom associated with the present model of case II transport. Without constraints on the magnitude of ϕ^* or $\tilde{\alpha}$, it is not possible to uniquely define the three transport parameters. In the present case

the dilation data for both PEMA and bituminous coal were fitted to characteristic case II curves, using $\tilde{\alpha}$ as a floating variable while ϕ^* was independently constrained. The final constraint used was the solvent front velocity, v, obtained from magnetic resonance microscopy.

A relationship between ϕ^* and solvent concentration was established by relating the change in free volume of the solvent–polymer system to contributions from the respective free volumes of polymer and solvent taken independently.[36] Essentially linear T_g suppression with concentration is observed at low solvent concentrations:

$$\Delta T = -k\phi_S \tag{13}$$

where $\Delta T = T_{g,supp} - T_{g,dry}$, k is typically in the range of 200–500 K for a variety of solvents,[36] and ϕ_S is the volume fraction of the solvent. Recalling that T_g of PEMA is only 308 K, the value of ϕ_S, accordingly, is anticipated to be very small. Using a lower value of k, we calculate ϕ_S = 0.05, yielding ϕ^* = 0.17. Bituminous coal is reported to have its T_g on the order of 650–700 K, suggesting that ϕ_S of pyridine must be very high. Indeed, calculations along these lines have indicated that ϕ_S (calculated) actually exceeds the equilibrium ϕ_S associated with coal dilated at room temperature at a solvent activity of 1.0.[24b] On the basis of this analysis, it would appear that pyridine is not capable of suppressing coal's T_g to less than room temperature, which is inconsistent with the present results. Recent experimental results derived from incremental solvent sorption isotherm experiments on bituminous coal, however, clearly indicate the presence of a glass transition at solvent activities of less than 1.0, yielding a magnitude of ϕ^* on the order of 0.65.[37]

The gross dilation behavior of both samples is clearly case II with an unambiguous sigmoidal uptake profile (Figure 8C,D). The essential character of the present model for case II transport processes is revealed when comparing the swelling kinetics of these two glassy networks. Both samples are essentially the same size, with uptake occurring over essentially the same interval of time. The glassy diffusion coefficients for the two samples are also very similar in magnitude. The coal's network relaxation rate following the glass transition, however, is almost 15 times larger (Table 2) than that of PEMA. It is the relative magnitudes of the critical concentration parameter, ϕ^*, which compensate for this disparity in the relaxation dynamics and result in comparable overall uptake times. For the case of PEMA swollen in methanol, ϕ^* is relatively small. In the present model, network relaxation at the glass transition drives diffusion; all other things remaining equal, the sooner relaxation occurs, the faster transport evolves.

Comparing all four samples, the nearly 2 order of magnitude difference in diffusion coefficients between the Fickian and case II systems is compensated by the lack of any phase-transition-induced, network relaxation in the Fickian systems. Generally, these results confirm assertions made by the authors of one of the earliest papers on the applications of magnetic resonance imaging to diffusion in glassy polymers;[5] i.e., it is the presence of the phase transition which drives the overall diffusion process.

Conclusion

The model presented in this paper quantifies non-Fickian behavior using a minimum number of parameters without sacrificing physical intuition for computational simplicity. Although the parameters are phenomenologically based, they still retain a physical basis; thus, correlations with physical and chemical structural parameters associated with a given network are possible. The results demonstrate that magnetic resonance microscopy is particularly useful for both qualitatively revealing the essential character of transport during the swelling process and, quantitatively, yielding front velocities which are crucial to the data analysis and parameterization. Future studies will focus on designing more precise analytical methods for the purpose of measuring uptake data. Employing a higher static magnetic field will improve the sensitivity of time-resolved magnetic resonance microscopy and allow us to investigate network relaxation in the presence of deuterated solvents.

Acknowledgment. This work was performed under the auspices of the Office of Basic Energy Sciences, Division of Chemical Sciences, U.S. Department of Energy, under Contract Number W-31-109-ENG-38.

References and Notes

(1) Alfrey, T. E.; Gurnee, E. F.; Lloyd, W. G. *J. Polym. Sci.* **1966**, *12*, 249.
(2) (a) Richman, D.; Long, F. A. *J. Am. Chem. Soc.* **1960**, *82*, 509. (b) Long, F. A.; Richman, D. *J. Am. Chem. Soc.* **1960**, *82*, 513.
(3) Hui, C.-Y.; Wu, K.-C.; Lasker, R. C.; Kramer, E. J. *J. Appl. Phys.* **1987**, *61*, 5129.
(4) Hui, C.-Y.; Wu, K.-C.; Lasker, R. C.; Kramer, E. J. *J. Appl. Phys.* **1987**, *61*, 5137.
(5) Mareci, T. H.; Dønstrup, M.; Rigamonti, A. *J. Mol. Liq.* **1988**, *38*, 185.
(6) Weisenberger, L. A.; Koenig, J. L. *Macromolecules* **1990**, *23*, 2445.
(7) Mansfield, P.; Bowtell, R.; Blackband, S. *J. Magn. Reson.* **1992**, *99*, 507.
(8) Maffei, P.; Kiéné, L.; Canet, D. *Macromolecules* **1992**, *25*, 7114.
(9) Brenner, D. *Fuel* **1985**, *64*, 167.
(10) Cody, G. D.; Botto, R. E. *Energy Fuels* **1993**, *7*, 561.
(11) Enscore, D. J.; Hopfenberg, H. B.; Stannett, V. T. *Polymer* **1977**, *18*, 793.
(12) Jou, D.; Camacho, J.; Grmela, G. *Macromolecules* **1991**, *24*, 3597.
(13) Thomas, N. L.; Windle, A. H. *Polymer* **1982**, *23*, 529.
(14) (a) Vrentas, J. S.; Duda, J. L. *J. Polym. Sci., Polym. Phys. Ed.* **1977**, *15*, 403. (b) Vrentas, J. S.; Duda, J. L. *J. Polym. Sci., Polym. Phys. Ed.* **1977**, *15*, 417.
(15) Jackle, J.; Frisch, H. L. *J. Polym. Sci., Polym. Phys. Ed.* **1985**, *23*, 675.
(16) Durning, C. J. *J. Polym. Sci., Polym. Phys. Ed.* **1985**, *23*, 1831.
(17) Durning, C. J.; Tabor, M. *Macromolecules* **1986**, *19*, 2220.
(18) Neogi, P. *AIChE J.* **1983**, *29*, 829.
(19) Neogi, P. *AIChE J.* **1983**, *29*, 833.
(20) Hopfenberg, H. B.; Frisch, H. L. *J. Polym. Sci., Part B* **1969**, *7*, 405.
(21) Vrentas, J. S.; Duda, J. L. *AIChE J.* **1975**, *21*, 894.
(22) (a) Cody, G. D.; Davis, A.; Hatcher, P. G. *Energy Fuels* **1993**, *7*, 455. (b) Cody, G. D.; Davis, A.; Hatcher, P. G. *Energy Fuels* **1993**, *7*, 463.
(23) Howell, J. M.; Peppas, N. A. *Fuel* **1987**, *66*, 810.
(24) (a) Sanada, Y.; Honda, H. *Fuel* **1966**, *45*, 295. (b) Lucht, L. M.; Larsen, J. M.; Peppas, N. A. *Energy Fuels* **1987**, *1*, 56. (c) Yun, Y.; Suuberg, E. *Prepr. Pap.—Am. Chem. Soc., Div. Fuel Chem.* **1992**, *37*, 856.
(25) Dieckman, S. L.; Gopalsami, N.; Botto, R. E. *Energy Fuels* **1990**, *4*, 417.
(26) Callaghan, P. T. *Principles of Nuclear Magnetic Resonance Microscopy*; Oxford Science Publications, Clarendon Press: Oxford, 1991.
(27) Darken, L. *Trans. AIME* **1948**, *174*, 184.
(28) Tanaka, T.; Hocker, L. O.; Benedek, G. B. *J. Chem. Phys.* **1973**, *59*, 5151.
(29) Tanaka, T.; Fillmore, D. J. *J. Chem. Phys.* **1979**, *70*, 1214.
(30) Landau, L. D.; Lifshitz, E. M. *Theory of Elasticity*; Pergamon Press: New York, 1959.
(31) Peters, A.; Candau, S. J. *Macromolecules* **1986**, *19*, 1952.
(32) Bastide, J.; Duplessix, R.; Picot, C.; Candau, S. *Macromolecules* **1984**, *17*, 83.
(33) Guggenheim, E. A. *Mixtures*; Oxford, 1952.
(34) Cohen, M. H.; Turnbull, D. *J. Chem. Phys.* **1959**, *31*, 1164.
(35) Hermans, P. H. *A Contribution to the Physics of Cellulose Fibers*; Elsevier: Amsterdam, 1948.
(36) Ferry, J. D. *The Viscoelastic Properties of Polymers*; John Wiley & Sons: New York, 1980.
(37) Green, T. Personal communication.